# Impact of clay mineralogy on the petrophysical properties of tight sandstones

Al-Kharra'a, Hamad S.; Wolf, Karl Heinz A.A.; AlQuraishi, Abdulrahman A.; Mahmoud, Mohamed A.; Deshenenkov, Ivan; AlDuhailan, Mohammed A.; Alarifi, Sulaiman A.; AlQahtani, Naif B.; Zitha, Pacelli L.J.; More Authors

**DOI**
10.1016/j.geoen.2023.211883

**Publication date**
2023

**Document Version**
Final published version

**Published in**
Geoenergy Science and Engineering

227 (2023) 211883

Contents lists available at ScienceDirect

Geoenergy Science and Engineering

journal homepage: www.sciencedirect.com/journal/geoenergy-science-and-engineering

# Impact of clay mineralogy on the petrophysical properties of tight sandstones

Hamad S. Al-Kharra'a [a,*], Karl-Heinz A.A. Wolf [a,**], Abdulrahman A. AlQuraishi [d], Mohamed A. Mahmoud [c], Ivan Deshenenkov [b], Mohammed A. AlDuhailan [b], Sulaiman A. Alarifi [c], Naif B. AlQahtani [d], Hyung T. Kwak [b], Pacelli L.J. Zitha [a,***]

[a] Delft University of Technology, Department of Geotechnology, Stevinweg 1, 2628 CN, Delft, the Netherlands
[b] Saudi Aramco, Dhahran, Saudi Arabia
[c] College of Petroleum Engineering and Geosciences, King Fahd University of Petroleum & Minerals, Dhahran, 34464, Saudi Arabia
[d] National Centre for Oil & Gas Technology, King Abdulaziz City for Science and Technology, Riyadh, Saudi Arabia

ARTICLE INFO

*Keywords:*
Pore size distribution
Kaolinite booklets
Filamentous illite
EOR
Tight sandstone reservoirs

ABSTRACT

A full petrographic and petrophysical characterization of tight sandstones has been conducted as part of ongoing study of Carbon Dioxide Enhanced Oil and Gas Recovery ($CO_2$-EOR/EGR) and $CO_2$sequestration. The main purpose of this study is to give novel perception into the interplay of the rock characteristics and fluid flow in tight formations, which are candidates for EOR/EGR processes (macroscopic sweep vs. microscopic displacement efficiency). To achieve this, several experimental techniques, including routine core analysis, X-ray diffraction (XRD), X-ray fluorescence (XRF), thin sections petrography, Scanning Electron Microscopy (SEM) and capillarity/pore size distributions by using Mercury Injection Capillary Pressure (MICP), Nuclear Magnetic Resonance (NMR), and Micro-Computed Tomography (Micro-CT), were conducted. Three tight sandstone rock samples (Bandera, Kentucky, and Scioto) were used in this work and particular attention was paid to the impact of clay content on rock's pore system and other petrophysical characteristics and hence fluids flow during production process.

Results indicate that the presence of fibrous illite clay acting as pore bridging in Bandera and Kentucky samples have blocked the overall micro-pore system causing a significant reduction in the micro-pore throat system to 36% in Bandera sand and 50.9% in Kentucky sample. On the other hand, absence of fibrous illite and the presence of illite platelets in the Scioto sandstone led to a clear preservation of the sample's micro-pore throat attributing to a total of 59.1% of the total pore throat system.

A new dimensionless number (dimensionless micro-pore throat modality) was established, defined as the ratio of micro-to macro-pore sizes. This shows that Scioto has the highest value of 1.44 implying that both macro- and micro-pore systems contribute to flow. Therefore, the mitigation of oil bypass from smaller pores should be a key criterion in selecting the proper recovery methods. Results show the effect of clay mineralogy on pore system considering a part of the physical and spatial properties the pore/grain framework of the tight sandstones.

## 1. Introduction

Tight reservoirs are one of the main types of unconventional resources (Berg, 1986; Caineng et al., 2015; Althani, 2021), categorized as shale, sandstone, or carbonate rocks with low permeability and porosity (Zou et al., 2012; Caineng et al., 2013; Ma et al., 2021). In the 1970's, the U.S government classified tight reservoirs as those with permeability values less than 0.1 mD in order to make well development eligible for

* Corresponding author.
** Corresponding author.
*** Corresponding author.
*E-mail addresses:* H.S.H.Alkharraa@tudelft.nl (H.S. Al-Kharra'a), K.H.A.A.Wolf@tudelft.nl (K.-H.A.A. Wolf), aqurishi@yahoo.com (A.A. AlQuraishi), mmahmoud@kfupm.edu.sa (M.A. Mahmoud), ivan.deshenenkov@aramco.com (I. Deshenenkov), Mohammed.Duhailan@aramco.com (M.A. AlDuhailan), salarifi@kfupm.edu.sa (S.A. Alarifi), nqahtani@kacst.edu.sa (N.B. AlQahtani), hyung.kwak@aramco.com (H.T. Kwak), P.L.J.Zitha@tudelft.nl (P.L.J. Zitha).

https://doi.org/10.1016/j.geoen.2023.211883
Received 1 August 2022; Received in revised form 30 March 2023; Accepted 3 May 2023
Available online 4 May 2023

federal-state tax credit (Holditch, 2006). The National Resources of Canada (NRC) defined tight oil reservoirs as petroleum resources producing economically via hydraulic fracturing techniques regardless of the type of lithology (National Resources Canada, 2012). Several researchers used porosity ($\varphi$) and permeability ($k$) as threshold cut-off to characterize tight reservoirs, where $\varphi < 10\%$ and $k < 0.1$ mD (Wang et al., 2015; Zhang et al., 2016). Flow behavior in tight reservoirs is complicated because of their pore system (bodies and throats) heterogeneity formed during depositional and diagenetic processes (Burley and Worden, 2003). Geological and petrophysical rock characterization can help understand the pore systems and thus enable a better description of the flow processes involved in the production operations (Nelson, 2009; Stroker et al., 2013). Although that many industry professionals and researchers classify tight reservoirs based on a permeability threshold of 0.1 mD, investigating the complex pore size distribution should be considered as an essential key in tight reservoirs classification. Spatial correlations of pore throats and bodies are most relevant parameters for permeability in tight rock characterization. Smaller throat sizes lead to higher capillary pressures obstructing the fluid mobilization (Alamdari et al., 2012; Zhao et al., 2018).

Pore throats and bodies are important factors in exploration and development plans, hence, rock's pore system measurements techniques such as MICP, Micro-CT scan, and NMR examinations are widely used in petrophysical analysis. However, each technique has its limitations when applied to tight rocks. Micro-CT scanning is a non-destructive method utilized in order to characterize and determine high-resolution images of pore systems. Nevertheless, small sample sizes have to be acquired to obtain higher resolution (Sakellariou et al., 2003). Several studies reported Micro-CT scanning of tight rocks with resolutions ranging from 5 to 8 μm, which enabled smaller grains and micro-pores to be recognized (Bultreys et al., 2016; Peksa et al., 2015). The MICP technique is commonly applied to obtain the distribution of pore-throat size of rock specimens. It estimates the distribution of pore volume by injecting mercury under elevated pressure into pore space. The volume of mercury that intrudes the pores is measured, while injection pressure gradually increases up to a maximum of 60,000 psi. Therefore, MICP works well in tight rocks as it is capable of measuring pore-throat size down to around 0.003 μm (Giesche et al., 2006; Comisky et al., 2011). It is noteworthy that MICP is a destructive technique with both environmental and health issues (Rice et al., 2014; Lu et al., 2017).

NMR method is widely used to estimate petrophysical properties such as permeability, porosity, pore volumes, and wettability (Marschall, 1995; Hinedi et al., 1997; Coates et al., 1999; Chen and Balcom, 2006; El-Husseiny and Knight, 2017; Jin et al., 2020). Wang et al. (2020) studied the distribution of pore sizes in a variety range of permeability values between 0.07 and 4450 mD and found that NMR estimated porosity values are in good correlation with helium porosity. Centrifuge and NMR techniques were utilized to estimate the connate water and pore fluid distributions for the Middle Bakken formation (Karimi and Kazemi, 2015). They observed that oil occupies larger pores while water tends to reside in smaller pores. Micro-CT and MICP techniques are limited to a laboratory scale, while NMR method is applied to determine the distribution of pore size at both field and laboratory scales (Callaghan, 1993; Prammer, 1994; Kenyon, 1997; Heaton et al., 2002; Westphal et al., 2005).

Oil and water contain adequate amounts of hydrogen nuclei. When a rock specimen holding hydrogen molecules is put inside NMR device, the protons in pore system are polarized by the magnetic field. An NMR signal is generated via introducing radio frequency (RF) pulse sequence (Carr and Purcell, 1954). Mathematical inversion, i.e., inverse laplace transformation, converts the measured NMR signals to the relaxation time ($T_2$) of rock sample (Song, 2001). The $T_2$ relaxation is defined as the period it takes the magnetic vector to depart from and return to the lowest energy level after NMR is applied under the excitement of RF field (Meiboom and Gill, 1958; Lyu et al., 2018). The $T_2$ relaxation is proportional to the fluid distribution in pores (Kleinberg et al., 1994; Howard, 1998; Baban et al., 2021) where larger pores will depict longer $T_2$ values and tiny pores will show shorter $T_2$ values, hence, the pore volumes of various pores can be analyzed. NMR measurement can determine fluid volumes of core samples by knowing the $T_2$ cut-off value. In order to estimate the $T_2$ cut-off for given sample, $T_2$ relaxation is measured before and after the drainage displacement process. The $T_2$ cut-off value is related to the rock mineralogy (Looyestijn, 2008; Rios et al., 2014; Elsayed et al., 2021). However, many studies (Miller et al., 1990; Murphy, 1995; Zhang et al., 2003; Adebayo et al., 2017) recommended using the standard cut-off value of 33 ms for sandstone samples resulting in misinterpretation of pore volumes and permeability values. Therefore, mineralogical composition has a vital role in the determination of a sandstone pore framework. A new work on the effect of mineralization on petrophysical properties of Fontainebleau sandstone found that the impact of quartz overgrowth reduces porosity and permeability (Al Saadi et al., 2017). They also showed that other minerals present such as accessory oxides, clays and feldspar have very minor effect on rock wettability, since they were mostly included in the quartz overgrowth.

Different types and abundances of clay material can bridge and even clog the pore networks preventing the fluid transport. In addition, distribution of the clays varies from reservoir to reservoir that makes 2D and 3D microscopy analysis of the core material a key factor for both successful oil and gas exploration and development campaigns (Zhu et al., 2020). The presence of clay minerals lowers the rock quality in sandstones, especially porosity and permeability (Neasham, 1977). Porosity and permeability reveal an inverse relationship with the total clay mineral content (Schrader and Yariv, 1990; Yuan et al., 2015). Rosenbrand et al. (2015) measured the permeabilities of Rotliegend sandstones; they believed that fibrous illite as demonstrated by SEM images, contributes to lower permeability. Kuila and Prasad (2013) found that kaolinite clay minerals reduce porosity in sandstone while it has less effect on permeability.

Previous works investigated the impact of clay minerals on pore structure in sandstone rocks (Stueck et al., 2013; Wang et al., 2020), nevertheless, detailed analyses of the effect of clay contents (type and size) on the micro-pore bodies and throats and relating them to the microscopic displacement efficiency of the micropore system in tight sandstone rocks are still not fully discussed. In this study, three representative tight sandstone samples were characterized. At the first stage, measurements and quantifications of the mineralogy accessory of three outcrops samples using several imaging tools (Micro-CT, XRD, SEM and petrographic thin-sections) are conducted. This multiple approach allows us to acquire mineral type and content at different resolutions. A set of experimental tests was performed by using a helium porosimeter, gas permeameter, MICP, NMR, and Micro-CT imaging, to determine key petrophysical parameters of the three sandstone samples and to establish the effect of clay mineralogy and contents on the pore framework of tight sandstone reservoirs. A new dimensionless parameter is established to characterize pore throat's heterogeneity and their control on fluids flow at different pore levels during the recovery processes in tight sandstones helping in better planning of such processes.

## 2. Materials and methodology

### 2.1. Core samples

Three outcrop sandstone samples were chosen as model to represent tight sandstone reservoirs. These are Bandera, Kentucky, and Scioto sandstones provided by Kocurek Industries company™, Caldwell, TX, US from different quarries (Fig. 1). These quarries are a good source for the construction industry and the rocks are known for their homogeneous characteristics suitable for comparable petroleum engineering laboratory tests (Farid Ibrahim and Nasr-El-Din, 2018; Hassan et al., 2019; Elsayed et al., 2021).

All samples originated during the Carboniferous, in a fluvial

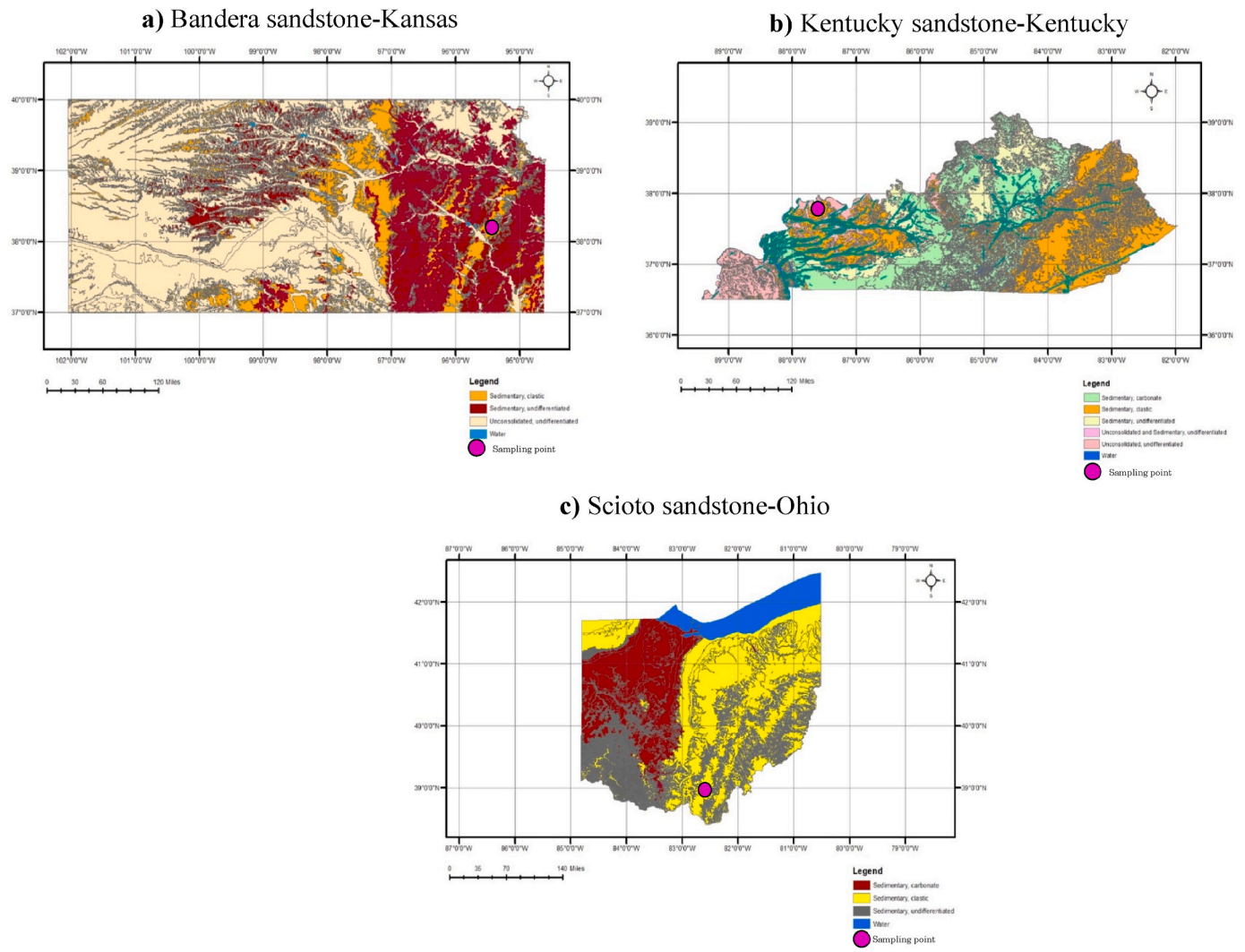


**Fig. 1.** Location of samples used in this study, where (a) Bandera sandstone, (b) Kentucky sandstone, and (c) Scioto sandstone (USGS, 2023).

depositional system with porosity reduction caused by their burial history. Bandera sandstone located in Southeastern Kansas and it is a member of Bandera shale formation that was deposited during the Desmoinesian age of the middle Pennsylvanian subsystem (323-299 Ma) (Adams et al., 1903; Jewett and Abernathy, 1945). It is a brown, thin-bedded sandstone, ranging from 0 to 10 m in thickness. The original fluvial depositional environment is fine-grained, and poorly-sorted (Martino, 1989; Brownfield et al., 1998; Koch and Burke, 2009).

Kentucky sandstone is light grey excavated from the western portion of the Kentucky Coal Field. It belongs to the Caseyville formation that was deposited during lower Pennsylvanian time (Glick, 1963; Gildersleeve, 1965; Shawe, 1966; Greb et al., 1992; Harris, 2007). Scioto sandstone samples were acquired from the Buena Vista member near McDermott, southern Scioto County, Ohio. This member is part of the lower Mississippian Cuyahoga formation covers the western part of Appalachian basin and has been deposited as deltaic turbidite deposits (Hull et al., 2004; Hannibal et al., 2006; Wolfe and Stucker, 2013). Scioto sandstone is blue grey, consisting of mostly coarse silt or fine sand and generally well-sorted (Saja and Hannibal, 2017). Stratigraphic divisions of the tested sandstones for this study (Fig. 2). When more samples are used, a detailed geological description would be significant for future studies involving reservoir rocks.

### 2.2. Experimental data collection and processing

Prior to the experiments, dry samples with radius of 3.8 cm and length of 4 cm were vacuumed for 2 day at 75 °C. Thereafter, plug samples were used to measure the permeability and porosity values at 20 °C. A Vinci™ helium porosimeter was used to determine the samples total connected porosity while Core-Lab™ gas permeameter was utilized to determine gas permeability and Klinkenberg liquid permeability. Subsequently, petrographical and morphological analysis of samples was conducted by using Micro CT, SEM, and thin-section imaging. Thin sections of ca. 3 $cm^2$ area were prepared from the end trim of the three sandstone plugs, that were examined, by using polarization microscopy to evaluate the mineralogy, mineral distribution, textures, and area porosity with a resolution down to 1 μm (Nichols, 2009; Ghiasi-Freez et al., 2012; Wardaya et al., 2013; Asmussen et al., 2015; Varfolomeev et al., 2016). Image J, an image analysis program, was applied to analyze and quantify the characteristics of the 2D images. A thin disk of circa 5 mm in thickness and a volume of ca. 10 $mm^3$ solid rock volume was then prepared for the three sandstones. To provide a higher resolution in the sub-nanometer range (Bultreys et al., 2016), TESCAN™ instrument (model MIRA3) equipped with EDX detector was used to generate SEM density images with a pixel resolution in nanometres to distinguish growth and interaction in and between mineral grains next to pore morphology (Doughty and Tomutsa, 1996; Ahmed, 2008). For spatial 3D texture quantification, Micro-CT scanning with a 3D X-ray

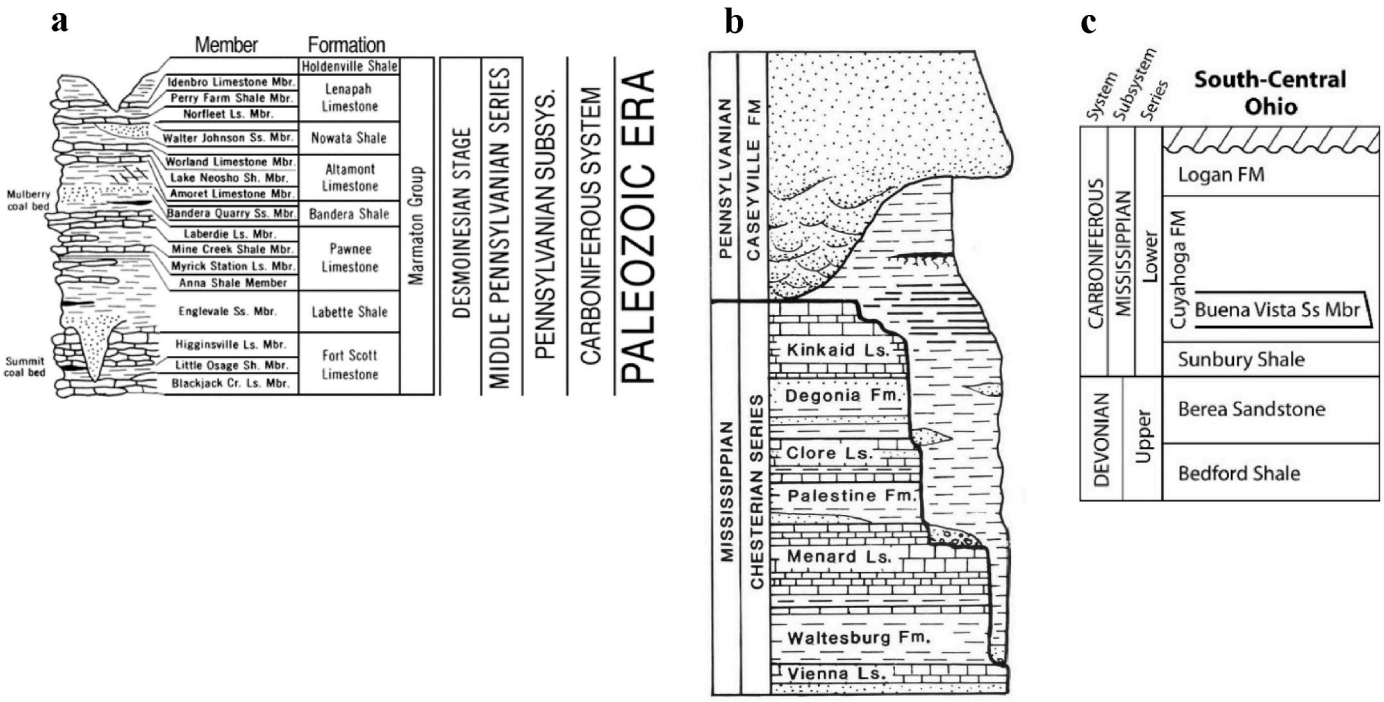


**Fig. 2.** Stratigraphic divisions of outcrop sections of (a) Bandera (Pepper et al., 1954), (b) Kentucky (Greb et al., 1992), (c) Scioto (Hull et al., 2004).

Microscope Zeiss Xradia Versa-620 was conducted on cylindrical plugs with a diameter of 4.3 mm and a length of 4.1 mm samples. The measurements were carried out by using a 100 KV/7 X-ray source, providing 5001 slices for rendering. The resolution of the Micro-CT depends on sample shape and volume; therefore, different size cylindrical plugs were prepared to obtain a 5-μm voxel size. Pore structure characterization was performed by using the maximum ball method (Buades et al., 2005; Dong et al., 2007). Table 1 lists the primary data of image spatial characteristics.

Elemental and mineralogical analyses (XRF and XRD measurements) were performed on grinded samples. XRF measurements were conducted using Rigaku™ NEX CG instrument with a maximum voltage of 40 kV and current of 1 mA. Data acquisition and elements evaluation was completed with QuantEZ software. XRD measurements were obtained with a Rigaku™ ULTIMA IV powder X-Ray diffractometer using a Cukα source at 40 kV and 40 mA with a 2θ-range of 3°–100° at 0.02° step size within 8 min time period.

NMR measurements were conducted using a 2 MHz Oxford Instruments GeoSpec 2–75 equipped with Green Imaging Technologies (v6.1) software. The NMR measurements were done by the Carr-Purcell-Meiboom-Gill (CPMG) pulse (Carr and Purcell, 1954). The main acquisition parameters used in these experiments are listed in Table 2. Three vacuumed samples saturated with 3% KCL brine were subjected to NMR measurements. KCL was used for preparing the brine because it is more compatible with sandstones than other common salts like NaCl and it was used in this work to mitigate any damage to rocks samples (Green et al., 2008; Elsayed et al., 2021). A Centrifuge at 4000 revolutions per minute (rpm) was then used to desaturate the samples with air as the displacing phase and another NMR measurements was conducted to determine the movable and immovable fluid volume. A Micrometrics Auto Pore V 9600 was used for mercury intrusion capillary pressure (MICP) analysis. MICP experiments were conducted to estimate the distribution of throat size via the drainage capillary pressure. The instrument measures pore throat diameters between 0.003 and 500 μm. In order to preserve the clay structure, the test was conducted on dry cylindrical 1.27 × 1.27 cm plugs at 75 °C at incremental injection pressures up to 60,000 psia (450 MPa).

**Table 1**
List of plug samples with corresponding dimensions and Micro-CT scan voxel size.

| Sample | Resolution (μm/voxel) | NY (voxel) | NX (voxel) | NZ (voxel) | Length size (mm) | Diameter size (mm) |
|---|---|---|---|---|---|---|
| Bandera | 5 | 761 | 828 | 836 | 3.81 | 4.14 |
| Kentucky | 5 | 709 | 717 | 715 | 3.55 | 3.59 |
| Scioto | 5 | 709 | 717 | 715 | 3.55 | 3.59 |

**Table 2**
Main parameters of NMR acquisition.

| Parameter | Value |
|---|---|
| Echo spacing time, TE | 110 μs |
| Signal to Noise Ratio, SNR | 150 |
| Total number of scans | 32 |
| Number of Echoes | 27,272 |
| Maximum $T_2$ | 300 ms |

## 3. Results

### 3.1. Porosity and permeability

The estimated permeability and porosity of investigated core

**Table 3**
Pore volume, porosity, and permeability values of core samples used for this study. All core samples have diameter of 3.8 ± 0.1 cm and length of 3.9 ± 0.1 cm.

| Sample | Pore volume (cc) | Porosity (vol%) | Permeability (mD) |
|---|---|---|---|
| Bandera | 10.1 | 24.4 | 24.12 |
| Kentucky | 6.8 | 15.0 | 0.98 |
| Scioto | 7.88 | 17.5 | 1.21 |

samples are listed in Table 3. The results indicate that Scioto and Kentucky have similar petrophysical properties with a porosity of 17.5 vol% and 1.2 mD for Scioto, and 15 vol% and 0.98 mD for Kentucky. Bandera sample shows a better reservoir quality of 24.4 vol% porosity and 24.12 mD permeability.

### 3.2. Petrography and mineralogy

Petrographic and mineralogy analyses were determined with thin-sections (Polarization microscopy), SEM and XRD techniques. SEM and thin-section results show that the Scioto sandstone contains moderately well sorted grains of medium silt to fine sand sizes of 30–120 μm (on average, 110 μm). The grain shape is subangular to subrounded and the grain contacts are predominantly point to face contacts. Based on point counting, the Scioto sample shows a visible intergranular porosity of 24% (Fig. 3a). The SEM micrographs revealed a pore-lining illite platelets coating quartz grains (Fig. 4a). Point counting (300 points) shows that Scioto's grain framework is composed of circa 44% quartz, 14% lithics, and <1% feldspar, where the rock fragments are composed of metamorphic and sedimentary rocks, with a minor amount of volcanic rock fragments. Based on the textural maturity classification by (Folk, 1951), Scioto's grains are subrounded and moderately sorted with low amount of clay content. Therefore, the sandstone can be classified as submature sublitharenite (Fig. 5, Folk, 1980; Boggs, 2012) (see Fig. 6).

The Bandera sandstone has a grain framework comprising of 64% quartz, 2% feldspars and 1% lithic fragments, indicating that the sandstones could be classified as quartzarenite, according to the triangle of Folk (Fig. 5). The rock fragments include metamorphic, sedimentary, and minor volcanic fragments. The mica contained 8% muscovite (with an average of 2.8%) and trace amount (<1%) of biotite. The particle size revealed that the Bandera is fine to very fine-grained, between 30 and 180 μm (averaging 87 μm), and moderately to well sorted. Grains are mainly sub-angular to angular and exhibit long grain contacts (Fig. 3b). Booklets of Kaolinite were recognized by SEM images with ranges of 5 μm to 10 μm in size (Fig. 4d). Such booklets can partially or completely reduce porosity in general and micro-porosity in specific.

Additionally, SEM images of Bandera sandstone shows clear kaolinite 'books' and filamentous illite overlying the quartz overgrowth (Fig. 4c). Visible pores between grains were clearly observed in thin-sections and SEM images (Fig. 1b and 2c), respectively.

Kentucky sandstone shows moderately to poorly sorted coarse silt-size grains of 55 μm on average. The grains are largely subangular to angular in shape with clay minerals filling spaces between grains indicating that the sample has a matrix supported fabric (Fig. 3c). SEM images demonstrate that fibrous illite act as pore bridging (average 0.25 μm wide). Due to the presence of fibrous illite, permeability is reduced by partial blockage of pore throats (Fig. 4b). The mineral phases in Kentucky consist of 58% quartz, 1% feldspars, 1% lithic fragments, and 20% mica. The grains contacts are long to concave-convex contact planes. Intergranular porosity of 14% was observed in thin-sections micro-pores have not been clearly recognized.

XRD and XRF results are summarized in Tables 4 and 5, respectively. The results show high percentages of quartz, 89.2, 77.1, and 64.2% for the Scioto, Kentucky, and Bandera sandstones, respectively. Bandera sandstone has a total clay content (illite, kaolinite, and chlorite) of 14.3%, while the total clay contents of Kentucky and Scioto sandstones are 3.6 and 4.1%, respectively with illite as the prevailed clay mineral in the tested core samples measuring 6.4%, 3.6% and 2.2% for Bandera, Kentucky, and Scioto, respectively (Fig. 4). The chemical index of weathering (CIW) has been determined by using Harnois equation (Harnois, 1988). Accordingly CIW values of tested sandstones were calculated based on XRF measurements as 67.04%, 51.89%, and 42% for Bandera, Kentucky, and Scioto samples, indicating that tested sandstones have undergone low chemical weathering conditions.

### 3.3. Petrophysical measurement

MICP, Micro-CT, and NMR analytical results were examined to investigate the impact of clay minerals on micro-pore bodies and throats. According to Nelson's pore system size distribution, micro-porosity is assigned to pore bodies smaller than 10 μm, and micro-pore throats have throat diameters larger than 1 μm. However, the macro-, and meso-pore systems are applied to pore bodies exceeding 30

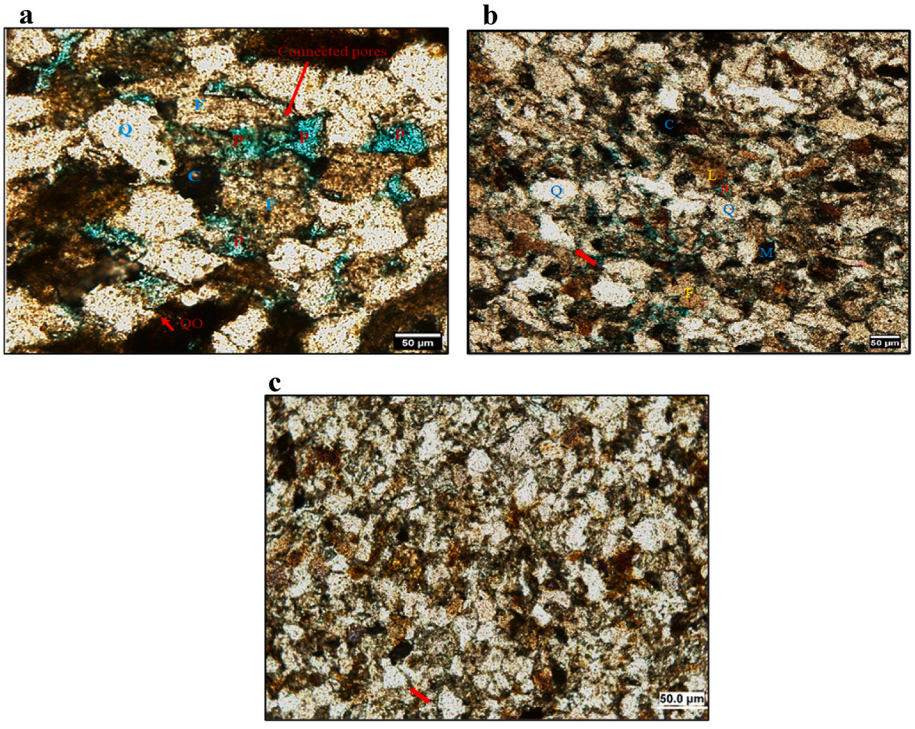


**Fig. 3.** Thin-sections showing the textural properties of Bandera, Kentucky, and Scioto sandstones. (a) Scioto exhibits coarse silt to fine-sized grains, lithics (L) illustrates as dirty brown colors, straight edges are the result of quartz overgrowths (QO) around elongated quartz grains (Q), weathering of a feldspar (F), dark color indicates matrix in the sample (M), and moderately visible pores between grains (P), (b) Bandera is fine grained sandstone, grain shape is angular to sub-rounded, well sorted sediments. Clearly visible primary pore spaces are clearly recognizable, Quartz overgrowth around original grains, (c) Kentucky is medium to coarse silt size with poorly sorting sediments, no visible pores between grains, some Quartz overgrowth around grains.

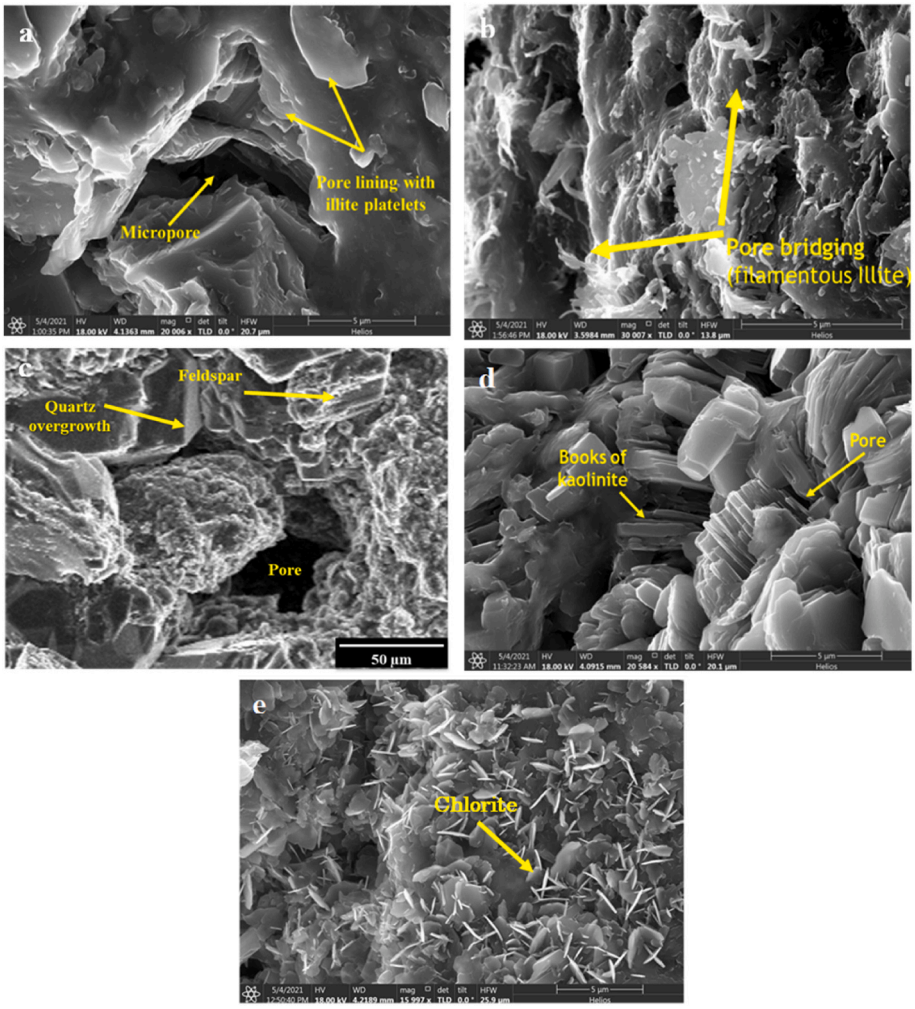


**Fig. 4.** SEM images represent (a) Scioto shows pore-lining with illite platelets and visible micro-pores, (b) Kentucky shows pore bridging with illite filamentous, (c) Bandera shows sharp surface as a result of the quartz overgrowths and visible pores between elongated grains, and top partly weathered feldspar with clays, (d) Kentucky shows books of kaolinite occluding pores, and (e) Bandera shows acircular chlorite filling micropores.

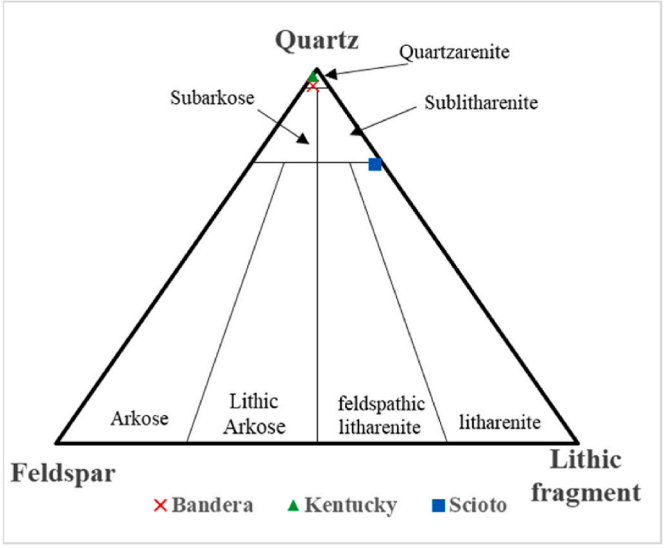


**Fig. 5.** Classification of sandstone after (Folk, 1980) criterion, where Bandera and Kentucky sandstones could be classified as quartzarenite, while Scioto sandstone can be named as sublitharenite.

µm and a throat diameter larger than 1 µm (Nelson, 2009). Micro-CT scan results were utilized to plot the pore size distribution versus their frequencies for the three sandstones (Fig. 7a). All sandstone samples show broader pore size spectrum with Bandera displaying relatively dispersed pore body distribution between 5 and 50 µm (averaging 24.4 µm). Kentucky and Scioto exhibit almost similar pore body size distribution with 5–28 µm (averaging 16.8 µm) for Kentucky, and 5 to 30 µm (averaging 18 µm) for Scioto. MICP-derived pore throat distributions are plotted in Fig. 7b. Bandera shows clear macro- and meso-pore throat systems with an average pore throat diameter of circa 6 µm. Kentucky and Scioto samples show narrower average throat sizes of approximately 1.8 µm.

Based on the micro-pore system criterion by (Nelson, 2009), the Scioto micro-pore throat and micro-pore body proportion results show the highest contribution to the total pore system with 59 vol% and 29.5 vol%, respectively. The Kentucky sandstone follows with a micro-pore throat and body contribution to the total pore system of 49 vol% and 23.5 vol%, respectively. The Bandera sandstone micro-pore throat and micro-pore body proportion shows the lowest contribution to the total pore system with 36 vol%, and 10 vol%, respectively (Fig. 7). To further investigate the pore systems and relate it to the previous results, NMR $T_2$ measurements were conducted "before and after" the centrifuge displacement test. $T_2$ cut-off values of tested sandstones were obtained as 17.8, 12.2, and 24.6ms for Bandera, Kentucky, and Scioto, respectively. Subsequently, these values were utilized to estimate the bound

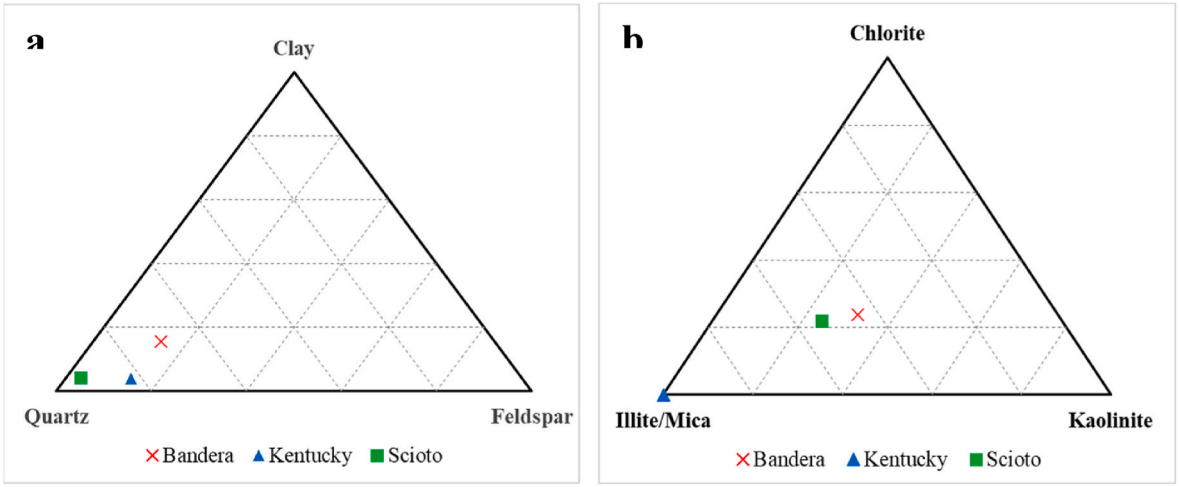


**Fig. 6.** Ternary diagrams of the tested sandstone samples, (a) represents minerals content and (b) shows clay minerals content.

**Table 4**
Mineralogical Compositions of Bandera, Kentucky, and Scioto sandstone samples (units in wt%).

| Sample | Quartz | Plagioclase | Orthoclase | Anhydrite | Ilmenite | Siderite | Dolomite | Halite | Hematite | Pyrite | Chlorite | Illite | Kaolinite |
|---|---|---|---|---|---|---|---|---|---|---|---|---|---|
| Bandera | 64.4 | 12 | 1 | 3 | 1 | 0.5 | 0.4 | 1.4 | 1.2 | 0.8 | 3.4 | 6.4 | 4.5 |
| Kentucky | 77.1 | 10.2 | 2.8 | 3.6 | 0 | 0.7 | 0.9 | 0.8 | 0.3 | 0 | 0 | 3.6 | 0 |
| Scioto | 89.2 | 2.1 | 0.7 | 3 | 0 | 0.2 | 0 | 0.2 | 0.5 | 0 | 0.9 | 2.2 | 1 |

**Table 5**
Elemental compositions of Bandera, Kentucky, and Scioto sandstone samples (units in wt%).

| Sample | $Al_2O_3$ | $SiO_2$ | $TiO_2$ | $Fe_2O_3$ | MnO | MgO | CaO | $Na_2O$ | $K_2O$ | $P_2O_5$ | $SO_3$ |
|---|---|---|---|---|---|---|---|---|---|---|---|
| Bandera | 4.93 | 79.90 | 0.49 | 3.02 | 0.86 | 1.16 | 1.50 | 0.92 | 0.71 | 0.12 | 1.87 |
| Kentucky | 2.88 | 88.25 | 0.59 | 0.81 | 0.13 | 0.31 | 1.91 | 0.76 | 0.83 | 0.05 | 1.81 |
| Scioto | 1.20 | 93.21 | 0.50 | 0.81 | 0.10 | 0.30 | 1.28 | 0.38 | 0.31 | 0.1 | 1.20 |

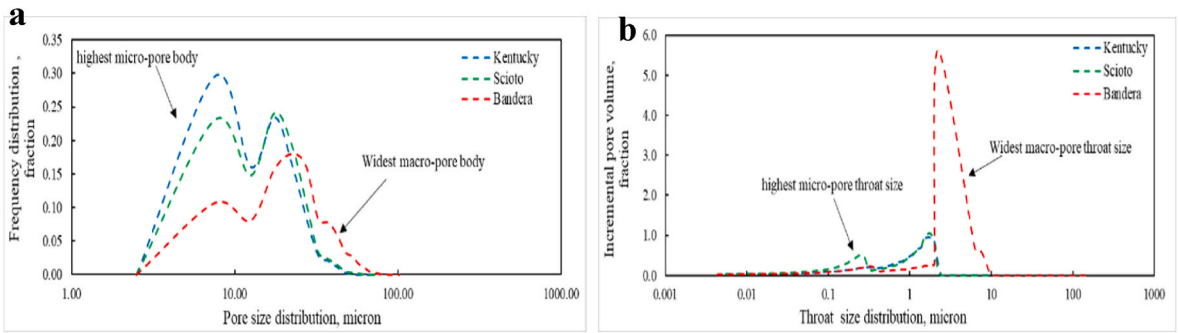


**Fig. 7.** Pore size and throat distributions of Bandera, Kentucky, and Scioto sandstones, where (a) shows pore-body diameter distributions obtained by Micro-CT scan and (b) represents pore-throat diameter distributions obtained with MICP.

volume index (BVI) and Free fluid index (FFI) of all pore frameworks. BVI is the cumulative NMR-porosity after centrifuge test, while FFI is fully saturated cumulative NMR-porosity minus BVI. NMR results show that Scioto has the highest bound fluid with almost 9% of the total porosity, while Kentucky shows the lowest value of bound fluid with 7.5% of the total porosity. Bandera sandstone exhibits the highest movable fluid among the three sandstones with 14.3% of the total porosity (Fig. 8).

## 4. Discussion

For the tight sandstones analyzed, we found that the porosity and permeability increase with the total clay mineral content (Fig. 9a and b), and this comes in line with findings of Lai et al. (2018) and Wang et al. (2020). To gain a deeper insight into the relationship of porosity, permeability, and clay minerals, it is more convenient to focus on the effect of clay contents on pore bodies and throats. Our study showed a relatively wider pore-throat size distribution in Bandera (24.4% porosity, 24.11 mD permeability) covering the micro-, meso-, and macro-pore throat systems with the highest total clay content of 14.3%. However, the significant contribution to flow mainly comes from the macro-pore throat system (64% macro-pore throat proportion) (Table 6). This macro-pore throat system accesses only the dominant macro-pore body system (89.4% pore body system proportion) as

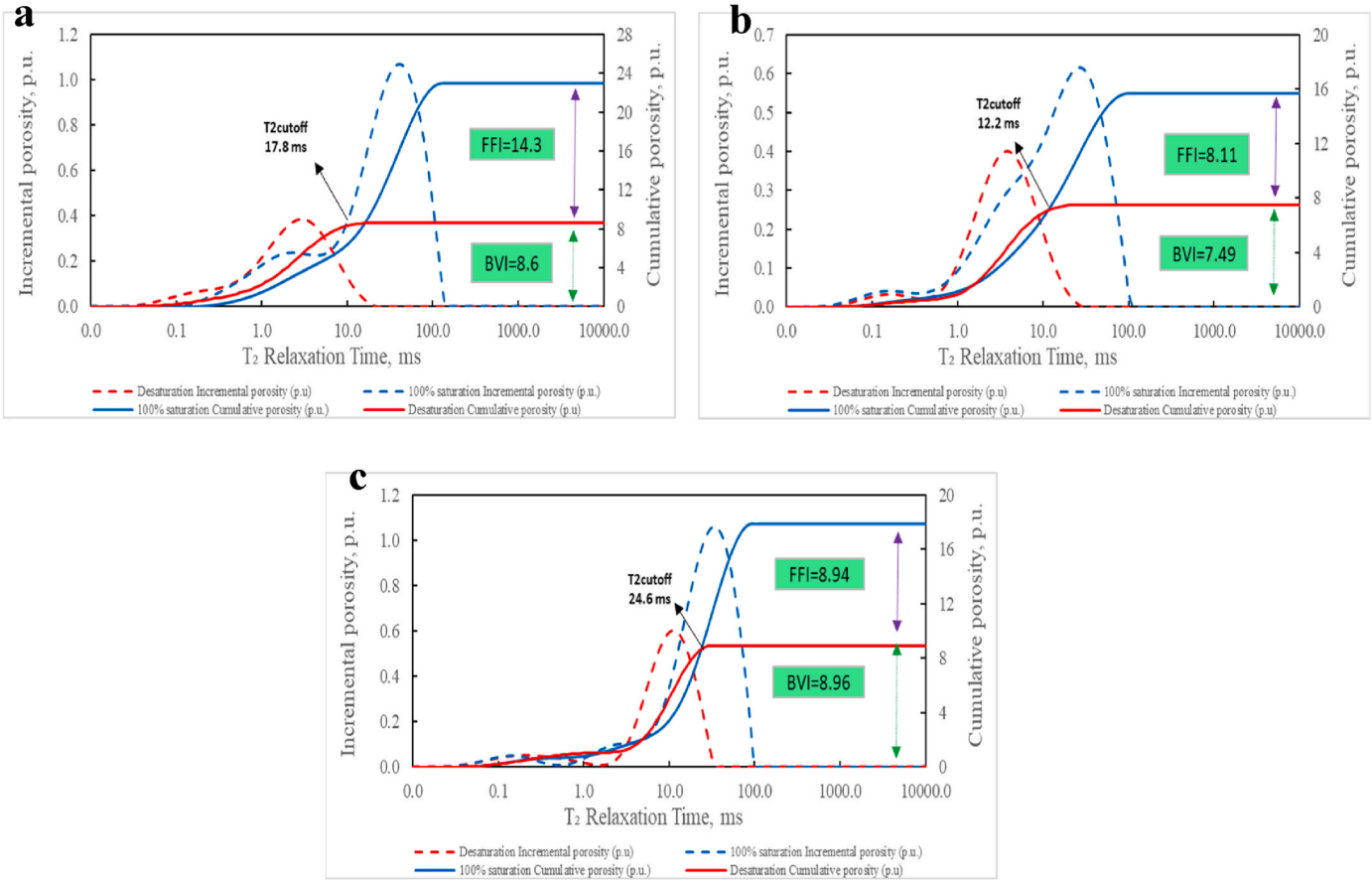


**Fig. 8.** $T_2$ relaxation measurements for three sandstone samples at fully brine saturation and after centrifuge displacement test: (a) Bandera, (b) Kentucky, and (c) Scioto Sandstone samples, where cumulative porosity at fully brine saturation (dark blue solid line), incremental porosity at fully brine saturation (dark blue dashed line), cumulative porosity post drainage with air (red solid line), and incremental porosity post drainage with air (red dashed line).

yielded from digital rock analysis. This finding is in contradiction with the study of (Wu et al., 2022), who stated that the lower the clay mineral content is, the larger pores can be found, and the more movable fluid content exist in the larger pore throats.

In contrast, this study displayed that the marked presence of the macro-pore system in Bandera, when compared to the other samples, can be ascribed to the absence of quartz overgrowth as a result of clay coating effect, and relatively larger grain size (average of 87 μm), which aligns with the observation of Al Saadi et al. (2017). The low contribution of the macro-pore system in Kentucky and Scioto is attributed to the smaller pore size characterizing these rocks average of 16 μm for Kentucky and 18 μm for Scioto. In addition, we found finer grain size (average of 55 μm for Kentucky and 59 μm for Scioto) compared to the Bandera sample that characterized with relatively higher pore and grain size values of 24 μm and 87 μm, respectively (Fig. 10a). Therefore, a higher macro-body size proportion contributes to higher porosity (Fig. 10b).

This study showed that micro-pore body proportion (Fig. 9c) or micro-throat proportion (Fig. 9d) increase with drop of the total clay mineral composition for all tested samples. This finding agrees with that of Wang et al. (2020); where they showed that the increasing percentage of clay minerals clearly decreases the pore throat distribution, porosity, and permeability of tight sandstone. However, we specifically showed that fibrous illite clay acting as pore bridging in sandstone tends to block the existing micro-throat system, affecting the flow displacement efficiency and illite content and micro-throat size proportion are strongly correlated ($R^2 = 0.9994$, Fig. 9f). This confirms that the low contribution of micro-throat system is attributed to illite-chocking and validates the hypothesis of this study. In contrast, there is a relatively fair correlation between illite content and micro-pore body proportion, revealing that changes in illite content have less influence on micro-pore body proportion ($R^2 = 0.6058$, Fig. 9e). The micro-pore body system of Bandera are measured to be the least among the samples with10.6% proportion to the total system and this is attributed to the presence of Kaolinite as pore filling (average size of 5.2 μm), which tends to fill pores and therefore reduces the micro-pore system significantly. On the contrary, micro-pore systems of Kentucky and Scioto show higher values with 50.1% and 59%, respectively. The kaolinite content and micro-pore body proportions show a strong correlation ($R^2 = 0.9827$, Fig. 9g). However, kaolinite and micro-throat size proportions relation reveals a weaker correlation compared to the micro-pore body proportion ($R^2 = 0.708$, Fig. 9h), indicating that the kaolinite has little effect on micro-throat radius in tight sandstone samples.

The above experimental outcomes are consistent with the micro-pore system contribution obtained from NMR results. It indicates that Scioto has the highest micro-pore system contribution, almost 50% of the total porosity. Kentucky follows with 48% and Bandera has the smallest micro-pore system of 38%, as indicated in Table 6. Furthermore, NMR measurements illustrate that macro-pore system is dominant in Bandera with almost 62% proportion, which are in agreement with high percentage of intergranular pores observed with thin sections (Fig. 3b). In addition, Micro-CT and MICP results confirm that Banderas' macro-pore body and throat system proportions are the highest among the tested samples with 89.4% and 64%, respectively. The difference of micro-pore bodies and throats proportions is related to the limitation of each technique, which should be a subjected for further future studies.

Due to the significant complication of the pore-throat systems in tight rocks, most of displacing fluid during the injection method will

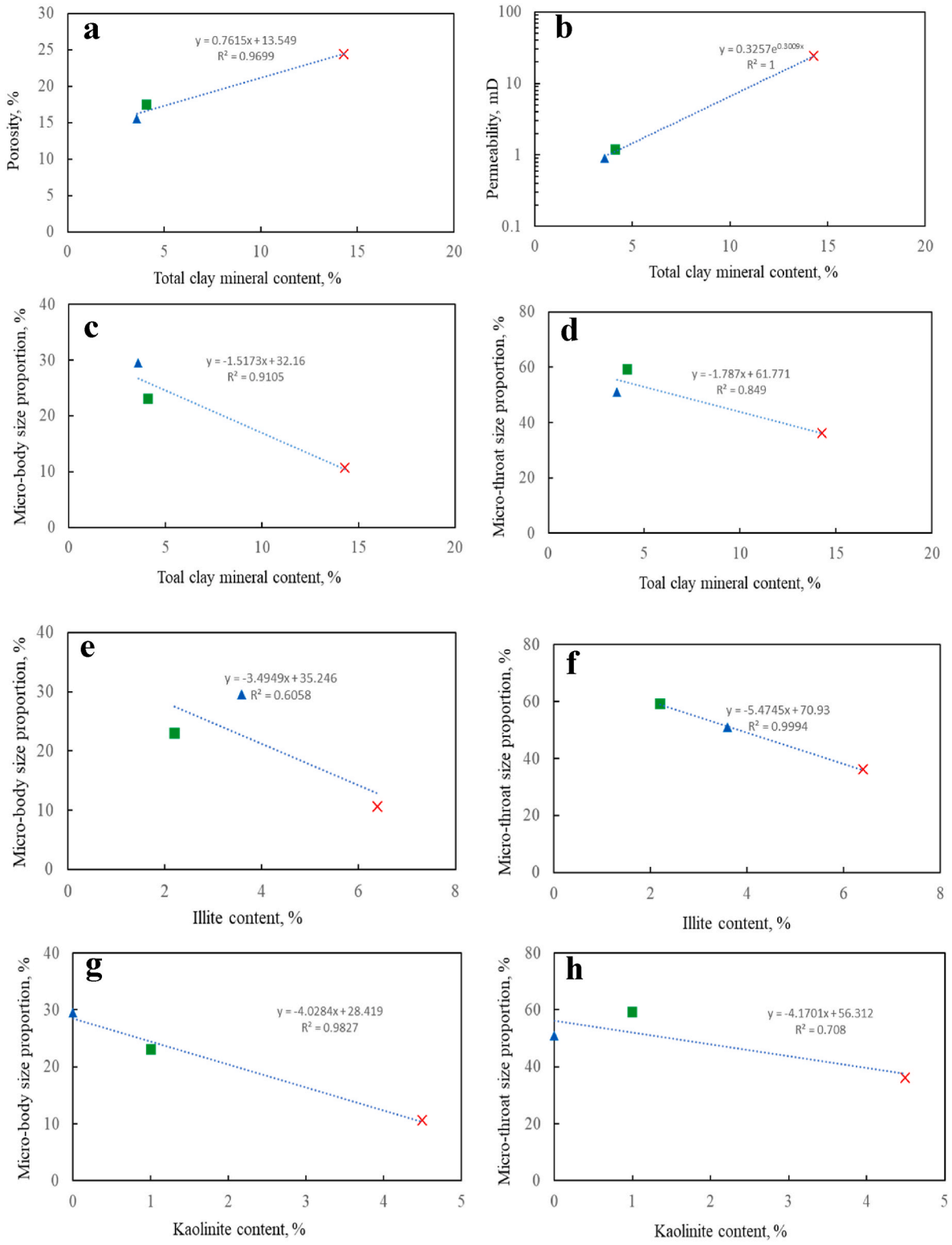


**Fig. 9.** Cross plots of clay mineral content and porosity, permeability, and proportions of micro-pore body size, micro-pore throat size. (a) the cross plots between total clay mineral content and porosity; (b) the cross plots between total clay mineral content and permeability; (c) the cross plots between total clay mineral content and micro-pore body size proportion; (d) the cross plots between total clay mineral content and micro-pore throat size proportion; (e) the cross plots between illite content and micro-pore body size proportion; (f) the cross plots between illite content and micro-pore throat size proportion; (g) the cross plots between kaolinite content and micro-pore body size proportion; (h) the cross plots between kaolinite content and micro-pore throat size proportion.

**Table 6**
Summary of the grain size, Micro-pore bodies and throats proportions, and micropore system of three sandstones samples.

| Sample | Average Grain size | Micro-pore body fraction (μCT) | Micro-throat fraction (MICP) | Micropore system fraction (NMR) | Micro-throat modality ratio (MTMR) |
|---|---|---|---|---|---|
| | (μm) | (%) | (%) | (%) | (fraction) |
| Bandera | 87 | 10.6 | 36 | 38 | 0.56 |
| Kentucky | 55 | 29.5 | 50.9 | 48 | 1.03 |
| Scioto | 59 | 23 | 59.1 | 50 | 1.44 |

favour the least resistant paths (macro-pore throat) and is going to bypass the displaced fluid in the micro-pore throat (Fig. 11). As a result, lower microscopic displacement efficiency of the injection process is faced due to channelling effect (Zhao et al., 2015; Madathil et al., 2015; Gao et al., 2016). The micro-pore throat modality ratio (MTMR) can be considered for describing the microscopic displacement efficiency of IOR/EOR processes. MTMR is a dimensionless number that relates the abundance size of the micro-pore throat to the macro-pore throat.

A large value of micro-pore throat modality ratio demonstrates that the most of the displacing fluid will flow mainly into the macro-pore throat leaving the micro-pore throat system behind. As a result, poor microscopic displacement efficiency occurs due to the inability of injected fluid to access the micro-pore system mobilizing the displaced fluid (Bolandtaba and Skauge, 2011; Lv et al., 2017).

(Fig. 12b) shows that kaolinite has little effect on MTMR, while illite reveals a strong negative correlation with MTMR ($R^2$ of 0.9774) in the tested sandstone samples (Fig. 12a). The results indicate that MTMR values decreases as illite content increases in sandstone samples, which negatively affects the microscopic displacement efficiency of tight sandstone. Therefore, high values of MTMR are needed to divert the displacing fluid using viscous fluids, foam, or polymer to reach out the oil residing in smaller pores and hence improving the microscopic displacement efficiency (Nguyen et al., 2014; Dong et al., 2016; Abdelaal et al., 2020).

The MTMR results were compared to NMR fluid parameters such as FFI/BVI (Kleinberg and Vinegar, 1996; Hinedi et al., 1997; Elsayed et al., 2021). The relationship confirmed that MTMR decreases as the ratio of movable to bound fluid increases in sandstone samples ($R^2$ = 0.8568, Fig. 13). Here the low MTMR value is ascribed to the high contribution of movable to bound fluid ratio confirming the hypothesis of this study. The bound fluid is reduced due to the presence of clay minerals that reduces the micropore contribution in tested samples. This novel micro-pore throat modality ratio (MTMR) is believed to be a key criterion in selecting the most efficient EOR methods in different tight sandstones. Larger dataset would offer further insight to our new dimensionless number which is a potential for future work based on these findings.

As indicated earlier, CIW values imply that tested sandstone samples exhibit low weathering conditions. The MTMR were compared to CIW values, and results showed a strong negative correlation ($R^2$ = 0.971, Fig. 14). For the tested samples, the MTMR decreases as CIW values increases, which suggests that the higher the CIW, the lower the flow contribution from micro-pore system, leading to a less overall microscopic displacement efficiency.

## 5. Conclusions

The primary goal of this study was to investigate the impact of clay minerals on the pore framework of tight sandstone samples and to relate it to the displacement efficiency. At the outset of this study, we proposed that illite clay acting as pore bridging could reduce the micro-throat system. Furthermore, we have argued that pore-filling kaolinite booklets could reduce micro-pore body system in tight sandstone. Finally, we have also hypothesized that the distribution of throats and bodies plays a significant role in the hydraulic properties of tight sandstone. The multi-techniques analysis reported has clearly supports the above hypotheses on how clay minerals affect pore structure, but needs to be placed in the context of the existing studies. Different tight sandstones were analyzed

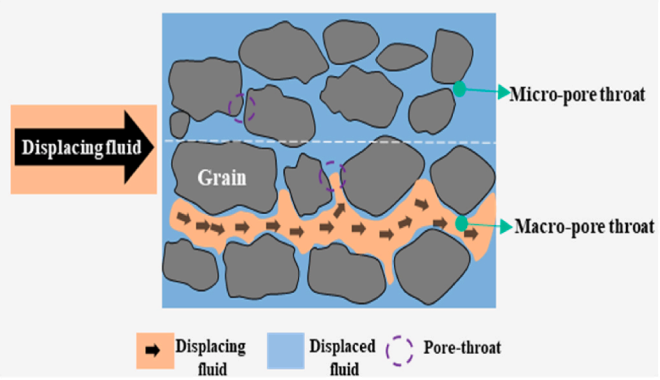


**Fig. 11.** Schematic showing that displacing fluid flows to the least resistance path (macro-pore throat) and bypasses the micro-pore throat area due to capillary effect.

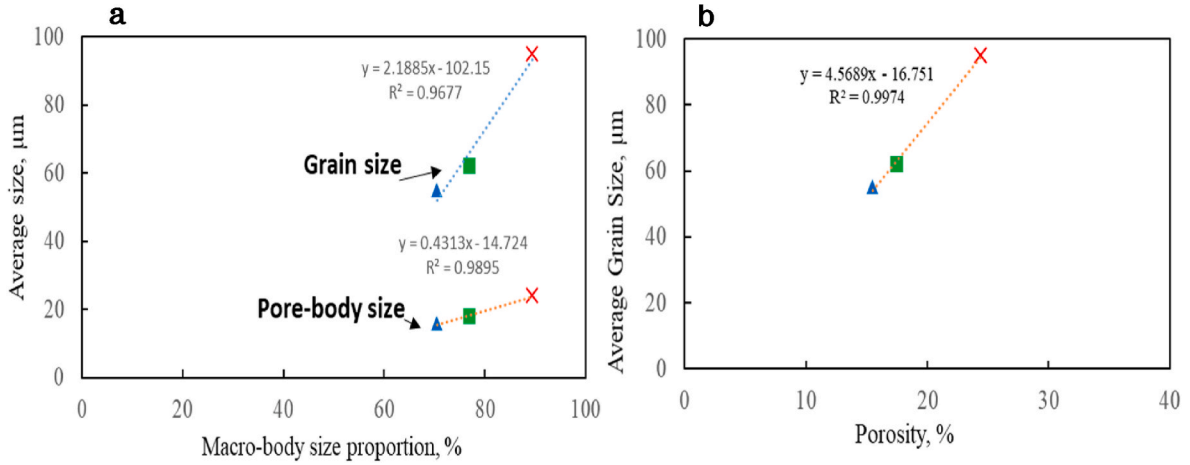


**Fig. 10.** Cross-plots showing the relation of macro-body proportion to the grain size, pore body size and porosity in tight sandstone samples. (a) Cross-plots showing the relation of macro-body proportion to the grain size and pore body size; (b) Cross-plots showing the relation of porosity to the grain size and pore body size.

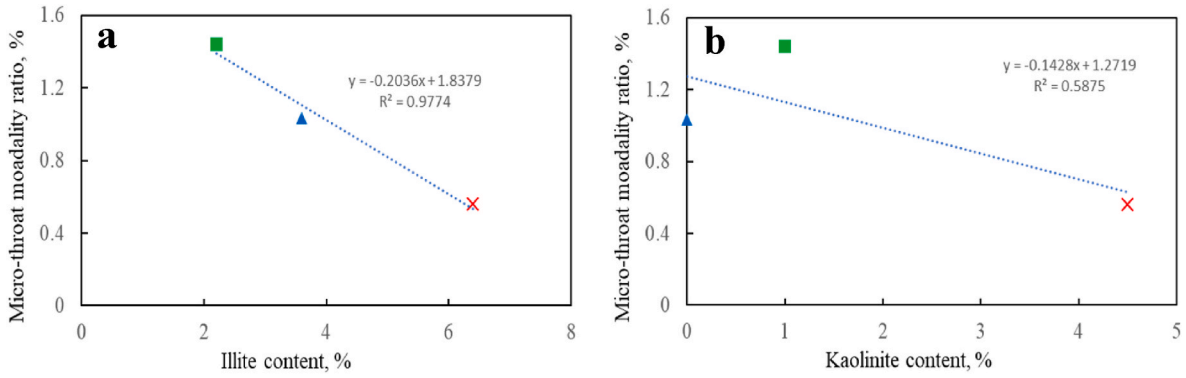


**Fig. 12.** Cross plots between MTMR against the content of illite, and kaolinite. (a) the cross plots between illite content and MTMR; (b) the cross plots between kaolinite content and MTMR.

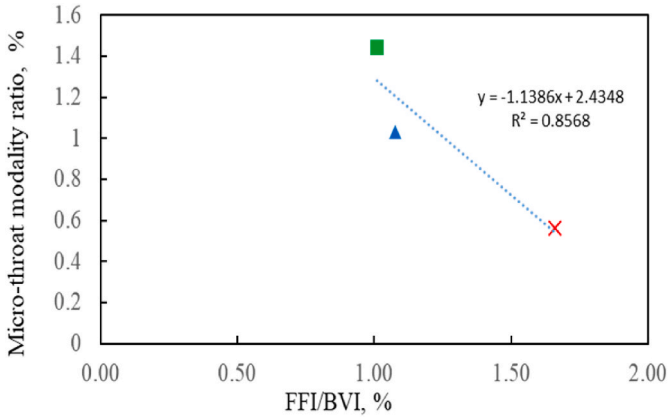


**Fig. 13.** Relationship between MTMR and the ratio of FFI/BVI.

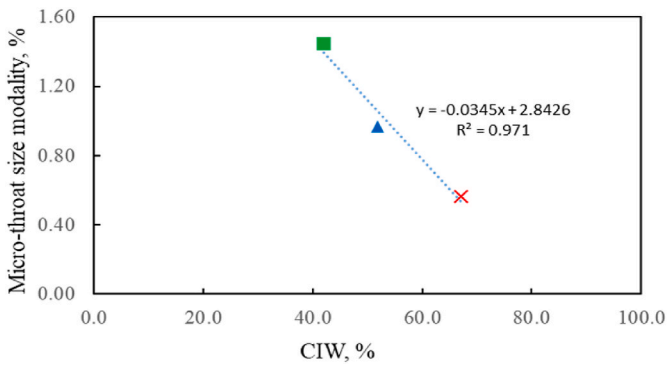


**Fig. 14.** Cross plot shows the relation between MTMR and CIW.

to define their petrography, mineralogy and petrophysical properties. Petrographic thin-sections, X-ray diffraction (XRD), X-ray fluorescence (XRF) and scanning electron microscopy (SEM) were used to determine the mineralogical and elemental composition; Mercury intrusion capillary pressure (MICP) experiments were used to define pore throat size distributions and nuclear magnetic resonance (NMR) and Micro-Computed Tomography Micro-CT measurements were utilized to determine the pore size distributions. Based on the multiple measurements conducted, the following can be concluded.

- Illite clay acting as pore bridging tends to reduce the micro-throat system. A strong correlation was obtained between illite content and micro-pore throat proportion in tested sandstone samples ($R^2$ = 0.9994) implying that the higher the illite content, the lower the micro-pore throat system proportion (36%, 50.9%, and 59.1% in Bandera, Kentucky and Scioto respectively.
- The presence of pore-filling kaolinite booklets reduces micro-pore body system in sandstone samples. Bandera characterized with 4.5 wt% kaolinite content shows low micro-pore body measured at 10.6 vol% of total pore body system. Nevertheless, the shortage of kaolinite clay minerals as the case in Kentucky and Scioto sandstones preserves the sample's total micro-pore body system (29.5 vol% and 23 vol%, respectively) revealing strong correlation ($R^2$ = 0.9827) between kaolinite content and micro-pore body proportion.
- The low contribution of macro-pore system in Kentucky and Scioto samples is attributed to finer grain size (55 μm and 59 μm in for Kentucky and Scioto, respectively), and smaller pore size (16 and 18 μm for Kentucky and Scioto, respectively). In contrast, Bandera shows a clear macro-pore representing 89.4% of total pore system due to the absence of quartz overgrowth as a result of clay coating, and relatively coarser grain size (87 μm).
- MTMR suggests that precaution should be taken in selecting the efficient recovery process for Scioto sandstone (1.44 MTMR) to mitigate the negative capillarity effect that can lead up oil bypass from the micro-throat system. Conversely, flow mostly comes from the macro-throat system for Bandera and oil bypass is minimal as indicated by MTMR of 0.56.
- A strong negative correlation was acquired between MTMR and CIW in tested sandstone samples, suggesting that the higher the CIW value, the lower the contribution of micro-pore throat system and hence the MTMR value.

## Credit author statement

**Hamad Al-Kharraa**: Writing, Organization, Experiments. **Karl-Heinz A.A. Wolf:** Supervision, Methodology, Investigation, Writing – review & editing. **Hyung T. Kwak**: Methodology, Resources, Data discussion. **Ivan Deshenenkov**: Resources, Investigation, Data Formal analysis. **Mohamed A. AlDuhailan:** Methodology, and Data discussion. **Mohamed A. Mahmoud**: Supervision, Methodology, Data discussion, Formal analysis. **Abdulrahman A. AlQuraishi**: Data investigation, Writing – review & editing. **Naif B. AlQahtani**: Data investigation and discussion, Resources. **Sulaiman A. Alarifi**: Data discussion and Writing – review & editing. **Pacelli L.J. Zitha**: Supervision, Project administration, Data discussion, Methodology, Writing – review & editing.

## Declaration of competing interest

The authors declare that they have no known competing financial interests or personal relationships that could have appeared to influence the work reported in this paper.

## Data availability

Data will be made available on request.

## Acknowledgments

The authors want to thank Dr. Ali AlYousef and Dr. Khaled Al Ramadan for their support of this study. Furthermore, we acknowledge the participation in the research organization and insightful conversations of Essa Abdullah, Mustafa Satrawi, Jun Gao, Dr. Abdulkareem Alradwan, and Hussain Al Ali. Special thanks extend to Dr. Saleh AlHaidary and Dr. Yasser AlDuailej for their valuable comments and suggestions.

## References

Abdelaal, A., Gajbhiye, R., Al-Shehri, D., 2020. Mixed CO2/N2 foam for EOR as a novel solution for supercritical CO2 foam challenges in sandstone reservoirs. ACS Omega 5 (51), 33140–33150.
Adams, G.I., Girty, G.H., White, D., 1903. Stratigraphy and Paleontology of the Upper Carboniferous Rocks of the Kansas Section (No. 211). US Government Printing Office.
Adebayo, A.R., Kandil, M.E., Okasha, T.M., Sanni, M.L., 2017. Measurements of electrical resistivity, NMR pore size and distribution, and x-ray CT-scan for performance evaluation of CO2 injection in carbonate rocks: a pilot study. Int. J. Greenh. Gas Control 63, 1–11.
Ahmed, W., 2008. Contrast in clay mineralogy and their effect on reservoir properties in sandstone formations. Bull. Chem. Soc. Ethiop. 22 (1).
Al Saadi, F., Wolf, K., Kruijsdijk, C.V., 2017. Characterization of Fontainebleau sandstone: quartz overgrowth and its impact on pore-throat framework. J. Petrol Environ. Biotechnol. 7 (328), 1–12.
Alamdari, B.B., Kiani, M., Kazemi, H., 2012. Experimental and numerical simulation of surfactant-assisted oil recovery in tight fractured carbonate reservoir cores. In: SPE Improved Oil Recovery Symposium. OnePetro.
Althani, M., 2021. Development potential of non-source tight-oil formations in the Middle East. In: Latin America Unconventional Resources Technology Conference. Unconventional Resources Technology Conference (URTEC), pp. 363–376, 16-18 November 2020.
Asmussen, P., Conrad, O., Günther, A., Kirsch, M., Riller, U., 2015. Semi-automatic segmentation of petrographic thin section images using a "seeded-region growing algorithm" with an application to characterize wheathered subarkose sandstone. Comput. Geosci. 83, 89–99.
Baban, A., Al-Yaseri, A., Keshavarz, A., Amin, R., Iglauer, S., 2021. CO2–brine–sandstone wettability evaluation at reservoir conditions via Nuclear Magnetic Resonance measurements. Int. J. Greenh. Gas Control 111, 103435.
Berg, R.R., 1986. Reservoir Sandstones. Prentice-Hall, Inc., Englewood Cliffs, NJ. Available from. https://www.osti.gov/biblio/5295813.
Boggs, S., 2012. Principles of Sedimentology and Stratigraphy.
Bolandtaba, S.F., Skauge, A., 2011. Network modeling of EOR processes: a combined invasion percolation and dynamic model for mobilization of trapped oil. Transport Porous Media 89 (3), 357–382.
Brownfield, R.L., Brenner, R.L., Pope, J.P., 1998. Distribution of the Bandera shale of the marmaton group, middle pennsylvanian of southeastern Kansas. Current Research in Earth Sciences 29–41.
Buades, A., Coll, B., Morel, J.M., 2005. A non-local algorithm for image denoising. In: 2005 IEEE Computer Society Conference on Computer Vision and Pattern Recognition (CVPR'05), vol. 2, pp. 60–65.
Bultreys, T., De Boever, W., Cnudde, V., 2016. Imaging and image-based fluid transport modeling at the pore scale in geological materials: a practical introduction to the current state-of-the-art. Earth Sci. Rev. 155, 93–128.
Burley, S., Worden, R., 2003. Sandston Diagenesis: Recent and Ancient. Reprint Serint Series Volume 4 of the International Association of Sedimentologists.
Caineng, Z., Zhang, G., Zhi, Y., Shizhen, T., Lianhua, H., Rukai, Z., Xuanjun, Y., Qiquan, R., Denghua, L., Zhiping, W., 2013. Concepts, characteristics, potential and technology of unconventional hydrocarbons: on unconventional petroleum geology. Petrol. Explor. Dev. 40 (4), 413–428.
Caineng, Z., Zhi, Y.A.N.G., Rukai, Z.H.U., Guosheng, Z., Lianhua, H., Songtao, W., Shizhen, T.A.O., Xuanjun, Y., Dazhong, D., Yuman, W., Lan, W., 2015. Progress in China's unconventional oil & gas exploration and development and theoretical technologies. Acta Geologica Sinica-English Edition 89 (3), 938–971.
Callaghan, P.T., 1993. Principles of Nuclear Magnetic Resonance Microscopy. Oxford University Press on Demand.
Carr, H.Y., Purcell, E.M., 1954. Effects of diffusion on free precession in nuclear magnetic resonance experiments. Phys. Rev. 94 (3), 630.
Chen, Q., Balcom, B.J., 2006. A single-shot method for capillary pressure curve measurement using centrifuge and quantitative magnetic resonance imaging. In: SPE/DOE Symposium on Improved Oil Recovery. OnePetro.
Coates, G.R., Xiao, L., Prammer, M.G., 1999. NMR Logging: Principles and Applications, vol. 234. Haliburton Energy Services, Houston.
Comisky, J.T., Santiago, M., McCollom, B., Buddhala, A., Newsham, K.E., 2011. Sample size effects on the application of mercury injection capillary pressure for determining the storage capacity of tight gas and oil shales. In: Canadian Unconventional Resources Conference. OnePetro.
Dong, H., Touati, M., Blunt, M.J., 2007. Pore network modeling: analysis of pore size distribution of Arabian core samples. In: SPE Middle East Oil and Gas Show and Conference. OnePetro.
Dong, X., Liu, H., Hou, J., Liu, G., Chen, Z., 2016. Polymer-enhanced foam PEF injection technique to enhance the oil recovery for the post polymer-flooding reservoir. In: SPE Western Regional Meeting. OnePetro.
Doughty, D.A., Tomutsa, L., 1996. Multinuclear NMR microscopy of two-phase fluid systems in porous rock. Magn. Reson. Imag. 14 (7–8), 869–873.
El-Husseiny, A., Knight, R., 2017. A laboratory study of the link between NMR relaxation data and pore size in carbonate skeletal grains and micrite. Petrophysics 58 (2), 116–125.
Elsayed, M., El-Husseiny, A., Kadafur, I., Mahmoud, M., Aljawad, M.S., Alqubalee, A., 2021. An experimental study on the effect of magnetic field strength and internal gradient on NMR-Derived petrophysical properties of sandstones. J. Petrol. Sci. Eng. 205, 108811.
Farid Ibrahim, A., Nasr-El-Din, H., 2018. Evaluation of the breakdown pressure to initiate hydraulic fractures of tight sandstone and shale formations. In: SPE Trinidad and Tobago Section Energy Resources Conference. OnePetro.
Folk, R.L., 1951. Stages of textural maturity in sedimentary rocks. J. Sediment. Res. 21 (3), 127–130.
Folk, R.L., 1980. Petrology of Sedimentary Rocks. Hemphill publishing company.
Gao, H., Li, T., Yang, L., 2016. Quantitative determination of pore and throat parameters in tight oil reservoir using constant rate mercury intrusion technique. J. Pet. Explor. Prod. Technol. 6, 309–318.
Ghiasi-Freez, J., Soleimanpour, I., Kadkhodaie-Ilkhchi, A., Ziaii, M., Sedighi, M., Hatampour, A., 2012. Semi-automated porosity identification from thin section images using image analysis and intelligent discriminant classifiers. Comput. Geosci. 45, 36–45.
Giesche, H., 2006. Mercury porosimetry: a general (practical) overview. Part. Part. Syst. Char. 23 (1), 9–19.
Gildersleeve, B., 1965. Geology of the Brownsville Quadrangle. Kentucky (No. 411).
Glick, E.E., 1963. Geology of the Clarkson Quadrangle, Kentucky: US Geol. Survey Geol. Quad. Map GQ-278.
Greb, S.F., Williams, D.A., Williamson, A.D., 1992. Geology and Stratigraphy of the Western Kentucky Coal Field.
Green, D.P., Dick, J.R., McAloon, M., Cano-Barrita, P.D.J., Burger, J., Balcom, B., Oaxaca, C.I.U., 2008. Oil/water imbibition and drainage capillary pressure determined by MRI on a wide sampling of rocks. In: SCA2008-01 Presented at the SCA Conference, vol. 29. UAE, Abu Dhabi.
Hannibal, J.T., Saja, D.B., Thomas, S.F., Hubbard, D.K., 2006. Quarrying history and use of Berea Sandstone in northeastern Ohio. In: Proceedings of the 42nd Forum on the Geology of Industrial Minerals, pp. 7–13.
Harnois, L., 1988. The CIW index: a new chemical index of weathering. Sediment. Geol. 55 (3), 319–322.
Harris, D.C., 2007. Kentucky consortium for Carbon storage. www.uky.edu.KGS/kyccs/ppt/071207_Harris.pdf.
Hassan, A., Mahmoud, M., Al-Majed, A., Al-Nakhli, A., 2019. New chemical treatment for permanent removal of condensate banking from different gas reservoirs. ACS Omega 4 (26), 22228–22236.
Heaton, N.J., Freedman, R., Karmonik, C., Taherian, R., Walter, K., DePavia, L., 2002. Applications of a new-generation NMR wireline logging tool. In: SPE Annual Technical Conference and Exhibition. OnePetro.
Hinedi, Z.R., Chang, A.C., Anderson, M.A., Borchardt, D.B., 1997. Quantification of microporosity by nuclear magnetic resonance relaxation of water imbibed in porous media. Water Resour. Res. 33 (12), 2697–2704.
Holditch, S.A., 2006. Tight gas sands. J. Petrol. Technol. 58 (6), 86–93.
Howard, J.J., 1998. Quantitative estimates of porous media wettability from proton NMR measurements. Magn. Reson. Imag. 16 (5–6), 529–533.
Hull, D.H., Larsen, G.E., Slucher, E.R., 2004. Generalized Columns of Bedrock Units in Ohio. State of Ohio, Department of Natural Resources, Division of Geological Survey.
Jewett, J.M., Abernathy, G.E., 1945. Oil and gas in eastern Kansas: Kansas Geo 1. Survey, Bull. 57, 245.
Jin, G., Xie, R., Xiao, L., 2020. Nuclear magnetic resonance characterization of petrophysical properties in tight sandstone reservoirs. J. Geophys. Res. Solid Earth 125 (2) e2019JB018716.
Karimi, S., Kazemi, H., 2015. Capillary pressure measurement using reservoir fluids in a middle bakken core. In: SPE Western Regional Meeting. OnePetro.
Kenyon, W.E., 1997. Petrophysical principles of applications of NMR logging. Log. Anal. 38 (2).
Kleinberg, R.L., Vinegar, H.J., 1996. NMR properties of reservoir fluids. Log. Anal. 37 (6), 20–32.
Kleinberg, R.L., Kenyon, W.E., Mitra, P.P., 1994. Mechanism of NMR relaxation of fluids in rock. J. Magn. Reson., Ser. A 108 (2), 206–214.
Koch, Z., Burke, C.D., 2009. Paleoenvironmental Interpretation of the Bandera Shale Formation, Marmaton Group, Desmoinesian Stage, Middle Pennsylvanian in Southeastern Kansas.
Kuila, U., Prasad, M., 2013. Specific surface area and pore-size distribution in clays and shales. Geophys. Prospect. 61 (2), 341–362.
Lai, J., Wang, G., Fan, Z., Zhou, Z., Chen, J., Wang, S., 2018. Fractal analysis of tight shaly sandstones using nuclear magnetic resonance measurements. AAPG (Am. Assoc. Pet. Geol.) Bull. 102 (2), 175–193.
Looyestijn, W.J., 2008. Wettability index determination from NMR logs. Petrophysics-The SPWLA Journal of Formation Evaluation and Reservoir Description 49 (2).

Lu, Q., Liu, Z., Chen, X., 2017. Mercury poisoning through intravenous administration: two case reports with literature review. Medicine 96 (46).
Lv, P., Wang, Z., Liu, Y., Dong, H., Jiang, L., Song, Y., Wu, B., Liu, S., 2017. Pore-scale displacement mechanisms investigation in CO2-brine-glass beads system. Energy Proc. 105, 4122–4127.
Lyu, C., Ning, Z., Wang, Q., Chen, M., 2018. Application of NMR T 2 to pore size distribution and movable fluid distribution in tight sandstones. Energy Fuel. 32 (2), 1395–1405.
Ma, T., Gui, J., Chen, P., 2021. Logging evaluation on mechanical-damage characteristics of the vicinity of the wellbore in tight reservoirs. J. Pet. Explor. Prod. Technol. 11 (8), 3213–3224.
Madathil, A., Azrak, O., Pearce, A., Al Amrie, O., Gunasan, E., Blondeau, C., 2015. 24 years of successful EOR through immiscible tertiary gas injection. November. In: Abu Dhabi International Petroleum Exhibition and Conference. OnePetro.
Marschall, D., Gardner, J.S., Mardon, D., Coates, G.R., 1995. Method for correlating NMR relaxometry and mercury injection data. September. In: 1995 SCA Conference, Paper, vol. 9511, p. 40.
Martino, R.L., 1989. Trace fossils from marginal marine facies of the kanawha formation (middle pennsylvanian), West Virginia. J. Paleontol. 63 (4), 389–403.
Meiboom, S., Gill, D., 1958. Compensation for pulse imperfections in Carr-Purcell NMR experiments. Rev. Sci. Instrum. 29, 688.
Miller, M.N., Paltiel, Z., Gillen, M.E., Granot, J., Bouton, J.C., 1990. Spin echo magnetic resonance logging: porosity and free fluid index determination. September. In: SPE Annual Technical Conference and Exhibition. OnePetro.
Murphy, D.P., 1995. NMR logging and core analysis–simplified. World Oil 216 (4), 65–68.
National Resources Canada, 2012. North American Tight Oil. http://www.nrcan.gc.ca/energy/sources/crude/2114#oil1.
Neasham, J.W., 1977. The morphology of dispersed clay in sandstone reservoirs and its effect on sandstone shaliness, pore space and fluid flow properties. In: SPE Annual Fall Technical Conference and Exhibition. OnePetro.
Nelson, P.H., 2009. Pore-throat sizes in sandstones, tight sandstones, and shales. AAPG Bull. 93 (3), 329–340.
Nguyen, D., Wang, D., Oladapo, A., Zhang, J., Sickorez, J., Butler, R., Mueller, B., 2014. Evaluation of surfactants for oil recovery potential in shale reservoirs. In: SPE Improved Oil Recovery Symposium. OnePetro.
Nichols, G., 2009. Sedimentology and Stratigraphy. John Wiley & Sons.
Peksa, A.E., Wolf, K.H.A., Zitha, P.L., 2015. Bentheimer sandstone revisited for experimental purposes. Mar. Petrol. Geol. 67, 701–719.
Pepper, J.F., de Witt Jr., W., Demarest, D.F., 1954. Geology of the bedford shale and berea sandstone in the Appalachian basin. Science 119 (3094), 512–513.
Prammer, M.G., 1994. NMR pore size distributions and permeability at the well site. In: SPE Annual Technical Conference and Exhibition. OnePetro.
Rice, K.M., Walker Jr., E.M., Wu, M., Gillette, C., Blough, E.R., 2014. Environmental mercury and its toxic effects. Journal of preventive medicine and public health 47 (2), 74.
Rios, E., Figueiredo, I., Machado, V., Compan, A., Santos, B., Trevizan, W., 2014. NMR relaxation time dependency on saturation and wettability of carbonate rocks. In: SEG Technical Program Expanded Abstracts 2014. Society of Exploration Geophysicists, pp. 612–617.
Rosenbrand, E., Fabricius, I.L., Fisher, Q., Grattoni, C., 2015. Permeability in Rotliegend gas sandstones to gas and brine as predicted from NMR, mercury injection and image analysis. Mar. Petrol. Geol. 64, 189–202.
Saja, D.B., Hannibal, J.T., 2017. Quarrying history and use of the Buena Vista freestone, south-central Ohio: understanding the 19th century industrial development of a geological resource. Ohio J. Sci. 117 (2), 35–49.
Sakellariou, A., Sawkins, T.J., Senden, T.J., Arns, C.H., Limaye, A., Sheppard, A.P., Sok, R.M., Knackstedt, M.A., Pinczewski, W.V., Berge, L.I., Øren, P.E., 2003. Micro-CT facility for imaging reservoir rocks at pore scales. October. In: 2003 SEG Annual Meeting. OnePetro.
Schrader, M.E., Yariv, S., 1990. Wettability of clay minerals. J. Colloid Interface Sci. 136 (1), 85–94.
Shawe, F.R., 1966. Geologic Map of the Reedyville Quadrangle. western Kentucky. No. 520).
Song, Y.Q., 2001. Pore sizes and pore connectivity in rocks using the effect of internal field. Magn. Reson. Imag. 19 (3–4), 417–421.
Stroker, T.M., Harris, N.B., Elliott, W.C., Wampler, J.M., 2013. Diagenesis of a tight gas sand reservoir: upper cretaceous mesaverde group, piceance basin, Colorado. Mar. Petrol. Geol. 40, 48–68.
Stueck, H., Koch, R., Siegesmund, S., 2013. Petrographical and petrophysical properties of sandstones: statistical analysis as an approach to predict material behaviour and construction suitability. Environ. Earth Sci. 69, 1299–1332.
USGS, 2023. Geological Maps of US States accessed March 29, 2023 at. https://mrdata.usgs.gov/geology/state.
Varfolomeev, I., Yakimchuk, I., Denisenko, A., Khasanov, I., Osinceva, N., Rahmattulina, A., 2016. Integrated study of thin sections: optical petrography and electron microscopy. October. In: SPE Russian Petroleum Technology Conference and Exhibition. OnePetro.
Wang, J., Feng, L., Steve, M., Tang, X., Gail, T.E., Mikael, H., 2015. China's unconventional oil: a review of its resources and outlook for long-term production. Energy 82, 31–42.
Wang, R., Shi, W., Xie, X., Zhang, W., Qin, S., Liu, K., Busbey, A.B., 2020. Clay mineral content, type, and their effects on pore throat structure and reservoir properties: insight from the Permian tight sandstones in the Hangjinqi area, north Ordos Basin, China. Mar. Petrol. Geol. 115, 104281.
Wardaya, P.D., Khairy, H., Sum, C.W., 2013. Extracting physical properties from thin section: another neural network contribution in rock physics. In: International Petroleum Technology Conference. OnePetro.
Westphal, H., Surholt, I., Kiesl, C., Thern, H.F., Kruspe, T., 2005. NMR measurements in carbonate rocks: problems and an approach to a solution. Pure Appl. Geophys. 162, 549–570.
Wolfe, M.E., Stucker, J.D., 2013. 2012 Report on Ohio Mineral Industries: an Annual Summary of the State's Economic Geology. Report to State of Ohio Department of Natural Resources Division of Geological Survey, p. 116.
Wu, K., Chen, D., Zhang, W., Yang, H., Wu, H., Cheng, X., Qu, Y., He, M., 2022. Movable fluid distribution characteristics and microscopic mechanism of tight reservoir in Yanchang formation, ordos basin. *Front. Earth. Sci. - PRC* 2022, *10*, 840875, DOI: 10.3389/feart.2022.840875.
Yuan, G., Gluyas, J., Cao, Y., Oxtoby, N.H., Jia, Z., Wang, Y., Xi, K., Li, X., 2015. Diagenesis and reservoir quality evolution of the eocene sandstones in the northern dongying sag, bohai bay basin, east China. Mar. Petrol. Geol. 62, 77–89.
Zhang, G.Q., Hirasaki, G.J., House, W.V., 2003. Internal field gradients in porous media. Petrophysics-The SPWLA Journal of Formation Evaluation and Reservoir Description 44 (6).
Zhang, X.S., Wang, H.J., Ma, F., Sun, X.C., Zhang, Y., Song, Z.H., 2016. Classification and characteristics of tight oil plays. Petrol. Sci. 13, 18–33.
Zhao, H., Ning, Z., Wang, Q., Zhang, R., Zhao, T., Niu, T., Zeng, Y., 2015. Petrophysical characterization of tight oil reservoirs using pressure-controlled porosimetry combined with rate-controlled porosimetry. Fuel 154, 233–242.
Zhao, X., Yang, Z., Lin, W., Xiong, S., Wei, Y., 2018. Characteristics of microscopic pore-throat structure of tight oil reservoirs in Sichuan Basin measured by rate-controlled mercury injection. Open Phys. 16 (1), 675–684.
Zhu, P., Dong, Y., Chen, M., Li, Z., Han, B., Wang, J., Cui, Y., 2020. Quantitative evaluation of pore structure from mineralogical and diagenetic information extracted from well logs in tight sandstone reservoirs. J. Nat. Gas Sci. Eng. 80, 103376.
Zou, C., Zhu, R., Liu, K., Su, L., Bai, B., Zhang, X., Yuan, X., Wang, J., 2012. Tight gas sandstone reservoirs in China: characteristics and recognition criteria. J. Petrol. Sci. Eng. 88, 82–91.